Proceedings of the ASME 2020 International Mechanical Engineering Congress and Expo
IMECE 2020
November 15-19, 2020, Portland, USA

IMECE2020- 23180

CAMERA-BASED COAXIAL MELT POOL MONITORING DATA REGISTRATION FOR LASER POWDER BED FUSION ADDITIVE MANUFACTURING

Yan Lu[1*], Zhuo Yang[2], Jaehyuk Kim[3], Hyunbo Cho[3,] and Ho Yeung[1]

1 National Institute of Standards and Technology
Engineering Laboratory
Gaithersburg, MD 20899
Email: [yan.lu, ho.yeung]@nist.gov

2 Pohang University of Science and Technology
Department of Industrial and Management Engineering
Pohang, Gyeongbuk 37673, Republic of Korea
Email: [jaehyuk.kim, hcho]@postech.ac.kr

3 University of Massachusetts Amherst
Department of Mechanical and Industrial Engineering
Amherst, MA 01003
Email: [zhuoyang]@engin.umass.edu]

ABSTRACT

The quality of powder bed fusion (PBF) built parts is highly correlated to the melt pool characteristics. Camera-based coaxial melt pool monitoring (MPM) is widely applied today because it provides high resolution monitoring on the time and length scales necessary for deep PBF process understanding, in-process defect detection, and real-time control. For such functions, MPM data has to be registered correctly to a well-defined coordinate system. This paper presents methods for camera-based coaxial melt pool monitoring (MPM) data registration using the build volume coordinate system defined in ISO/ASTM52921, for both open architecture AM systems and 3rd party MPM augmented closed commercial systems. Uncertainties are evaluated for the proposed methods and case studies provided to demonstrate the effectiveness of the methods.

Keywords: Additive manufacturing, Data registration, Machine learning, Melt pool monitoring, Powder bed fusion,

1. INTRODUCTION

Laser powder bed fusion (LPBF) is a type of additive manufacturing (AM) that uses a laser beam to melt and fuse material powder layer by layer. Metal LPBF processes involve the spreading of a thin layer of metal powder followed by exposure to high-intensity laser energy directed in scanned trajectories defined by digital models. Both shapes and properties of a material are formed out of the repetitive processes. The metal powder bed fusion process is complicated and stochastic by nature, involving multiple physical phenomena: heat absorption, melt pool formation, solidification, and even re-melting and re-solidification [1]. Investigating melt pool behavior, in both temporal and spatial domains, plays a critical role in understanding and controlling the physical phenomena [2]. However, melt pool behavior is particularly difficult to monitor because of the small size, roughly 50 μm to 250 μm wide, and rapid change, with melting and cooling occurring over approximately 10 μs to 100 μs [3].

Two types of melt pool monitoring (MPM) are reported: machine vision-based and photodetector-based. The former includes both coaxial and off-axial setups of cameras, while the latter measures radiative emission using a photodiode or a pyrometer. This paper focuses on camera-based coaxial melt pool monitoring systems. This type of monitoring can generate high resolution images, with the melt pool remaining nominally stationary within the field of view, at a high sampling rate. It provides an attractive

solution to monitor melt pool for deep process understanding, in-process defect detection, and real-time control [4].

Studies have found that melt pool characteristics, including both temperature and geometry, are highly correlated to as-built part structure and properties [5]. Some other studies aim to identify various factors that affect melt pool formation. The factors include processing parameters such as laser power and scan velocity, as well as environmental parameters such as chamber temperature and humidity [6].

Both types of studies aim to derive the relationships between metal PBF process parameters, melt pool characteristics, and material structure and properties. A large volume of design data, in-process control data, melt pool measurement data, as well as post structure inspection data, are collected and analyzed to identify or validate such relationships. These data are generated from various measurement devices or software systems at different AM development stages and hence represented in different spatial reference coordinate systems. For example, AM design data are based on abstract object space models, usually with a reference plane and the build orientation defined. The process controls are prescribed using the machine reference frame, defined by the galvo scanner's positioning of the laser in LPBF, while the actual laser beam positions can be sensed using encoders. Non-Destructive Evaluation (NDE) based post inspection data has its own reference frames depending on the part location and setup, as well as the scanning configurations. To have a meaningful correlation of melt pool characteristics to process controls or post inspected structure requires transforming all the data into a neutral/standard reference frame or coordinate system. This spatial alignment process is called data registration. Melt pool measurement data registration is a process to assign every melt pool observation to a geometric location in a selected coordinate system, and furthermore to map every pixel of each melt pool image to the right location. The latter is necessary to quantify melt pool size and shape as well as spatter and plume phenomena for part defect prediction.

Based on ISO 20005 [7], data registration is defined as a process of transforming different sets of data into one coordinate system [7]. This is a necessary step for multi-sensor fusion and collaborative information processing. Sensor modeling and calibration are the basis for sensing data registration. For camera-based sensing systems, various camera models can be built to map an image pixel to a real-world coordinate. The mathematical relationship can be calculated using the camera's intrinsic and extrinsic parameters [8]. If a camera's optical setup is complicated, e.g., a coaxial melt pool monitoring imaging system, the camera model can be obtained through a homography mapping using calibration data [9]. In medical applications, image data registration is defined beyond pixel mapping, usually referring to feature-based methods to find correspondence between image features such as lines and contours [10]. A deep-learning-based data registration method was also proposed to allow more complex data set to be aligned, like conceptual models as well as 3D datasets [11].

In the AM domain, multiple studies are reported ~~about~~ on camera-based coaxial MPM data collection and calibration. Zhirnov et al. reported a study to locate the position of the laser spot with respect to the imaged melt pool [12]. Research from NIST has resulted in several complete data sets with both control commands and process monitoring data, including ~~the~~ images captured by a coaxial high-speed camera [13, 26 and 27]]. The studies describe a melt pool monitoring system for an open architecture AM system, and data sets generated. However, neither of them addressed a systematic way to register the melt pool images to allow for process-structure-property correlation. A closed AM system with melt pool monitoring built on top of a commercial AM machine was described in [14]. Their data analysis and derived predictive model were limited to layerwise statistics because the melt pool images were acquired by an external MPM system, and the images were not registered to the local positions. No research work has been reported on data registration for this type of melt pool monitoring system, which are 3rd party addons to commercial AM systems.

This paper intends to fill the gap by introducing data registration methods for camera-based coaxial melt pool monitoring of powder bed fusion AM processes. First, we present a generic melt pool monitoring image data registration procedure with a formal problem definition. Second, we present data registration algorithms for both open architecture AM systems and closed AM systems with 3rd part MPM additions. For both cases, each image frame is first registered against its corresponding laser beam spot position. Then individual pixel registration is performed based on the relative distance of a pixel to the melt pool center. For a closed AM system, the data acquisition of the MPM system is not synchronized with the AM machine positioning system. Hence the laser beam position for each melt pool image frame is not available and has to be estimated. In this study, we explored the most advanced machine learning algorithms and solved the closed-system melt pool position estimation problem. Uncertainties are evaluated for the proposed methods, and case studies are provided to demonstrate the effectiveness of the methods.

The paper is organized as the following. Section 2 presents the build volume coordinate systems defined by ISO/ASTM52921 [28] and formulates the data registration problem. Section 3 presents the data registration method for open architecture systems. Section 4 describes the camera-based coaxial MPM data registration for commercial AM systems with augmented 3rd party process monitoring. Section 5 summarizes the paper with discussions and future work.

2. MPM DATA REGISTRATION OVERVIEW

In this section, we introduce the reference coordinate system used for in-situ data registration, formulate the camera-based coaxial MPM data registration into two problems, and define a general procedure to solve the problems. We also define two typical scenarios for solving the problem: data registration for

open architecture AM systems and data registration for closed AM systems.

2.1 A Reference Coordinate System

There are multiple coordinate system types defined in manufacturing practices, for example, machine coordinate system, work piece coordinate system, and tool coordinate system. All of them are "right-handed" three-dimensional Cartesian coordinate systems well defined by ISO 841 [15] and ISO 2806 [16]. For AM, ISO/ASTM 52921:2013(E) defines a build platform coordinate system. The build facing surface of the build platform is defined as the X-Y plane, and the center of this surface is the origin, named *build volume origin* in Figure 1. The build volume origin is different from the machine origin, as defined by the original equipment manufacturer, usually named as *Machine Zero*. In addition, this definition may not coincide with the galvo-based coordinate origin. The X-axis is defined parallel to the front of the machine and is horizontal and parallel with one of the edges of the build platform. The Y-axis runs perpendicular to the X-axis and parallels to the other edges of the build platform. The Z-axis runs normal to the building facing surface, pointing to the build orientation. For our study, instead of using continuous values for the Z-axis, we define Z-coordinates as a set of discrete layer numbers *{1,2,…N},* from the first layer to the last layer N.

Since the build platform coordinate system has a priority for AM applications , we adopt this definition as our reference coordinate system for melt pool monitoring data registration.

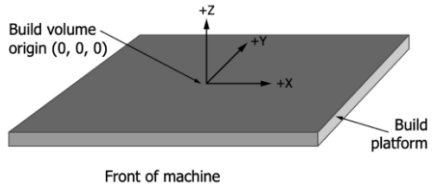

Figure 1: A reference coordinate system defined based on ISO/ASTM 52921

With the defined coordinate system, any point on the build surface for a specific layer process can be represented as *(x, y, n),* where *x* and *y* are confined by the build volume, and *n* is limited by the maximum layer number for any given layer thickness settings.

2.2 MPM Data Registration Problems and Procedure

The data generated from a camera-based coaxial MPM system includes layerwise time series of melt pool images, which can be represented as $F_{m,n}$, where *n* represents the corresponding layer number when the series of images are taken, and *m* represents the index of the frame in that time series. Assuming the pixel window size of the camera is *W*x*H*, then any given pixel *(i, j)* of the image frame $F_{m,n}$ can be represented as $(Px_i, Py_j)_{m,n}$, where $i=1…W$ and $j=1…H$.

Thus, a camera-based coaxial MPM data registration method is needed to solve two problems:

Problem 1: For any melt pool image $F_{m,n}$, find the corresponding laser beam location $(x_{m,n}, y_{m,n})$

Problem 2: For any pixel *(i, j)* of the $F_{m,n}$, named $(Px_i, Py_j)_{m,n}$, find the corresponding build volume coordinate location $(x_i, y_j)_{m,n}$.

Figure 2(a) and (b) illustrate the two problems, respectively. A solution to Problem 1 is required for data visualization and qualitative data fusion, for example, classifying and clustering melt pools based on the size or shape and correlating the results with porosity measurements. Problem 2 has to be solved if one needs to measure the absolute size of a melt pool or locate and quantify the phenomena of spatter and plume. More process features can be extracted based on Problem 2 solutions.

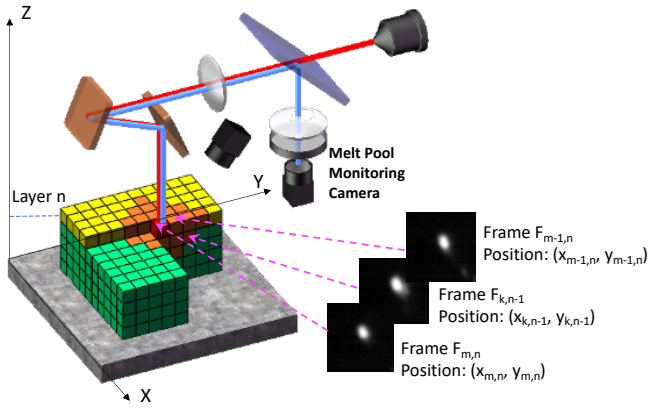

(a)

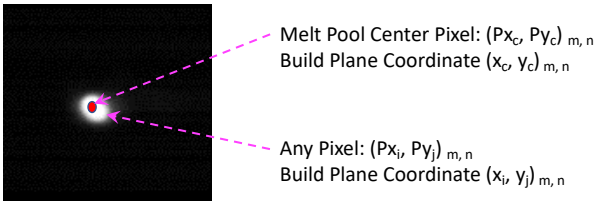

(b)

Figure 2: Camera-Based Coaxial MPM Data Registration Problems - Registering an image frame (a) Individual image registration (b)

With the problems formulated aforementioned, a general procedure for the camera-based coaxial MPM data registration can be identified, including 5 Steps.

Step 1: Registering Sensor Information – during this phase, all the sensor related information required by the data registration algorithms should be collected. In general, the sensor information can be classified into three categories: sensor parameters, reference frame information, and/or camera calibration data. How the optical path is designed decides how to calculate the spatial resolution (iFoV) for each image.

Step 2: Acquiring, Cleaning, Archiving, and Indexing images – this phase focuses on collecting images, treating missing data or contaminated data, storing and labeling melt pool

images frame by frame, layer by layer, using the index mechanism defined in Problem 1.

Step 3: Locating Image Frame – during this phase, a solution to Problem 1 is found. Every image frame for each layer is registered to a location on the build surface based on the coordinate system defined by ASTM.

Step 4: Locating Melt Pool Center – melt pool center is defined as the pixel within the MPM image that coincides with the center of the laser spot. The laser spot center may not coincide with the centroid of the melt pool image [12].

Step 5: Registering Melt Pool Image – this step assigns a build surface position to any pixel of a melt pool image, based on the relative pixel distance to the melt pool center and the pixel spatial resolution.

Steps 1 and 2 are relatively trivial. However, data preprocessing is a very important step. Images acquired should be scanned for missing frames or corrupted melt pool measurements. Melt pool no-shows on part contours or hatch regions indicate faults. Missing frames by camera or data transfer errors should be marked before data registration. Step 3 to 5 are challenging due to the dynamic nature of PBF processes and the complexity of MPM measurement setups, as well as the various latencies characterizing data acquisition systems. This paper focuses on solving the two MPM data registration problems needed for Step 3 to 5.

We address the problems in two different scenarios of AM system settings. Their given conditions are different; hence the solutions are different. In the first scenario, an open AM system is considered. An open system allows full control of laser scans as well as synchronized data acquisitions. For example, the NIST AMMT system uses a real-time controller to set galvo position and laser power as well as trigger acquisition of MPM images [17]. Another example is the GE Open Architecture system, which employs two embedded systems for open control and process monitoring separately [18]. The second scenario is more common where an AM system is built based on a closed AM machine with one or more 3rd party melt pool monitoring systems. The 3rd party melt pool monitoring data acquisition is independent of the AM system motion and laser control [14]. In this case, the associated laser beam center position for every image frame has to be estimated from the melt pool image characteristics.

3. OPEN ARCHITECTURE PBF SYSTEM CO-AXIAL MPM DATA REGISTRATION

3.1 Method Overview

Two types of open architecture AM systems were mentioned in Section 2. First is a custom-built system with full control of AM processes and data collection for melt-pool monitoring [17]. The melt pool data and laser spot positions from this type of system can be aligned using the camera triggers embedded in xy2-100 formatted build commands. The delays between the command signals and measured signals should be calibrated and removed for the temporal alignment. The second type of open architecture system doesn't have synchronized positioning and camera triggering commands to align the smart camera-generated timestamps with the encoder positions acquisition [18]. However, the delay between the two systems is constant, and it can be estimated based on a synchronized laser power measurement. This section illustrates a frame registration method for the first case, while it can be easily simplified for the second case.

Equation (1) shows a temporally aligned data matrix of scan commands, real measurement, and the camera control trigger based on xy2-100 format [19]. The first and last columns are the time stamp and camera control trigger, respectively. The synchronization of these two columns can guarantee the data of each row to be fully aligned. Columns 2 to 4 are the original scan command. Columns 5 to 7 are the measured scan position. Note, for multi-layers data; each layer has its corresponding matrix.

$$\begin{bmatrix} T_1 & x_1^{COM} & y_1^{COM} & P_1^{COM} & x_1^{MEA} & y_1^{MEA} & P_1^{MEA} & Tr_1 \\ T_2 & x_2^{COM} & y_2^{COM} & P_2^{COM} & x_1^{MEA} & y_2^{MEA} & P_2^{MEA} & Tr_2 \\ \vdots & \vdots & \vdots & \vdots & \vdots & \vdots & \vdots & \vdots \\ T_i & x_i^{COM} & y_i^{COM} & P_i^{COM} & x_i^{MEA} & y_i^{MEA} & P_i^{MEA} & Tr_i \\ \vdots & \vdots & \vdots & \vdots & \vdots & \vdots & \vdots & \vdots \end{bmatrix} \quad (1)$$

Figure 3 shows an example of a time series of scan command and the corresponding real scan position. It is noted that the real scan position is not identical to the scan command

1) The measured position is noisy compared to the command
2) The inertia of a galvo scanner is substantial compared with the sample rate. However, the delay can be measured. [17]

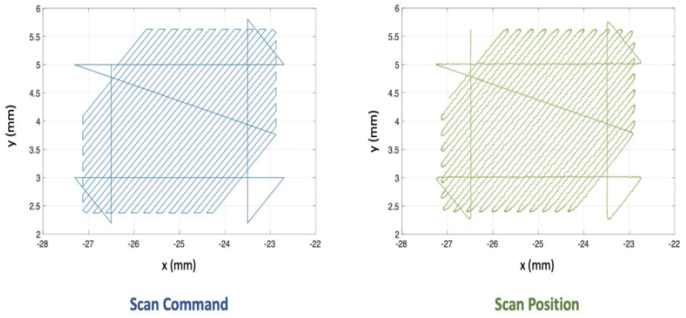

Figure 3: Scan commands vs. real scan positions

3.2 Image Frame Registration Against Laser Spot Position

The synchronized time stamps and camera triggers can be used to register the image frame against the laser spot position in the build platform coordinate system. Each image frame firstly is paired with its trigger command, and the laser position command correspondingly. However, it is preferred to register the melt pool with the real position measurement as it provides the most accurate spatial correlation with the as-built part and the Computer-Aided-Design (CAD) model. In order to perform that, a delay measurement must be conducted during the galvo calibration process. Assuming that the control and position

measurement sampling rate is T_s, the delay between the scan command and the scan position is t_{d1}, and the delay between the triggering command and the camera shutter opening is t_{d2}, Column 4-6 in Matrix (1) should be moved up for $(t_{d1}\text{-}t_{d2})/T_s$ rows to align actual laser beam positions with melt pool images.

After that step, at T_{rm} of layer n, image frame $F_{m,n}$ would be registered to point $[x_m^{MEA}, y_m^{MEA}]_n$ defined in the ISO/ASTM 52921 build coordinate system.

3.3 MPM Image Pixel Registration

In Section 3.2, each image frame is registered as a geometric point with no area, which completes Step 3, as defined in Section 2.2. This registered information can help the user to investigate the general melt pool conditions over the part. However, the image frame registration cannot provide enough details such as melt pool overlapping between tracks or a prediction of lack of fusion defects. To achieve this goal, each MPM coaxial image needs to be registered to the build platform coordinate system to provide a pixel-to-build plane projection.

For coaxial image systems, the imager is optically aligned with the laser beam such that the field of view moves with the laser spot. Consequently, nominal stationary melt pool images are obtained. The image window size is unchanged during the scan process. However, the pixel size could vary when the laser moves from the center of the build plane to the edge of the build platform, due to the distortion and stretching caused by perspective distortion from the location dependent, non-orthogonal viewing angles to the build plane [20, 21]. Research shows the real laser spot size is elongated when the laser beam shot on the build plate, not perpendicularly [21]. The pixel size calibration over the build platform is requested before the registration process.

To simplify this issue, the build platform can be divided into $k \times k$ grids, where each grid should cover a maximum area with minimum deflection angle change. Larger build platform results in larger deflection angle change, thus demands a larger k. Since each grid represents an area with a very small deflection angle range, it is reasonable to assume the pixel size is the same within one grid. If the part placed on the intersection area of multiple grids, the calibration would use the average size of the grids. It is assumed that $N_{xp}\ \mu m \times N_{yq}\ \mu m$ is the calibrated real pixel size for grid *(p, q)*, where x and y represent the pixel stretching direction.

Figure 4 shows an example of a gridded build plane, where the red area represents the hypothetical pixel distortion in different grids for illustration purposes. The specified iFoV is located in the center grid. The stretching ratio depends on the distance from the current grid to the center grid and the corresponding laser/camera view angle . The gray rectangle represents a $3\,mm \times 2\,mm$ test part placed at this location, referring to the example in Section 3.4.

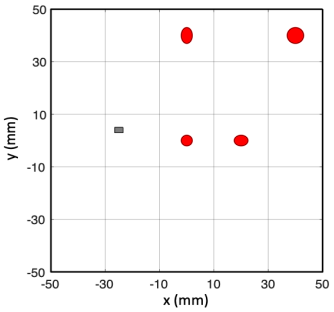

Figure 4. Pixel calibration grid for a build plane

Normally, both melt pools and laser spots cover more than one pixel area. The registration of a melt pool image assumes the center of a melt pool is perfectly mapped to the center of the laser spot. In this case, the center of the melt pool in an image frame should be identified and would be registered to the laser spot position first. The pixel located at the center of the area with the highest temperature is assumed to be the laser spot center [12]. After the center pixel$(P_{x_c}, P_{y_c})_{m,n}$ for $F_{m,n}$ is located, that pixel is registered to the position $[x_m^{MEA}, y_m^{MEA}]$, which was identified in Step 3. The center pixel then can be used as the reference to register the remaining pixels. To register any pixel (i, j) of that image, the grid should be identified for this image frame, as (p, q). Using a lookup table, the pixel size is found as $N_{xp}\ \mu m \times N_{yq}\ \mu m$. Then, $(P_{xi}, P_{yj})_{m,n}$, the pixel at (i, j) in the image, should be registered at

$$[x_m^{MEA} + (P_{xi} - P_{xc})N_{xp},\ y_m^{MEA} + (P_{yi} - P_{yc})N_{yq}] \qquad (2)$$

3.4 An Image Registration Example of AMMT

This section presents an example of the image frame and pixel registration based on the AMMT open platform [17]. The experiment builds a $3\,mm \times 2\,mm$ single layer part from IN625 powder located as marked in Figure 4. The experiment uses an orthogonal skywrite scan pattern with a constant laser power 195 W and a scan speed 800 mm/s. The part was built by 24 646 timestamps with 10 µs time interval. The coaxial camera is triggered every 50 µs to collect 1497 image frames. There is no laser input and image collected at the overshooting area. During the experiment, the encoder measures the real scan position.

Table 1 lists the fully aligned data of the first 6 time stamps. It roughly shows a 40 µs signal delay and a 0.05% position error. As shown in the table, the first image frame was captured at the beginning of the scan at the start point [-26.487 mm, 4.9985 mm].

Table 1. XYPT command for galvo, laser and camera control

Time Stamp	Scan Commands			Real Measurement			Camera Control
T_i (µs)	X_{COM} (mm)	Y_{COM} (mm)	P_{COM} (W)	X_{MEA} (mm)	Y_{MEA} (mm)	P_{MEA} (W)	Tr
0	-26.50	5.000	195	-26.487	4.9985	195	2
10	-26.50	4.992	195	-26.484	4.9985	195	0
20	-26.50	4.984	195	-26.484	4.9985	195	0

30	-26.50	4.976	195	-26.484	4.9985	195	0
40	-26.50	4.968	195	-26.484	4.9870	195	0
50	-26.50	4.960	195	-26.489	4.9704	195	2

Figure 5 shows the image frame registration result. The top plot shows the scan path and trigger position of the scan commands. The bottom plot shows the real position measured by the encoder. Both plots use the build platform coordinate system. Three sample coaxial images are marked in red, blue, and green frame. The corresponding timestamp is 28260 µs, 82620 µs, and 109410 µs, respectively. Both plots mark the trigger position by solid black dots. The figure extracts three example frames and marks their registered point on the plots. Each colored frame is registered to the point of the same color.

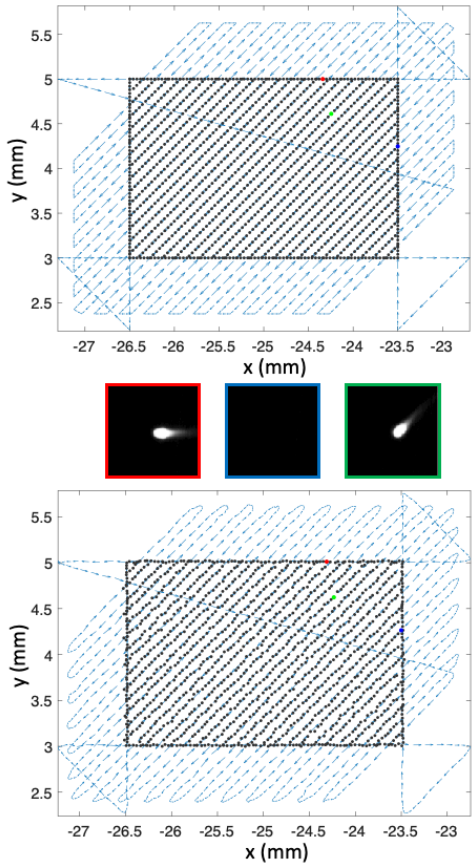

Figure 5. Image frame registration against scan command (top) and real measurement (bottom)

For AMMT, the distance from the build platform (100 mm x 100 mm) to the galvo is 500 mm. The laser beam deflection range is thus between -5.7° to 5.7°. According to the pixel size of AMMT coaxial image, 8 µm x 8 µm, the maximum distorted pixel is 8.04 µm x 8.04 µm. As a result, this example divides the build plane into a 5x5 grid, where the pixel size within one grid is assumed to be the same. For this build, the pixel would keep the original size in the y-direction and stretch in the x-direction. The calibrated pixel size is 8.0064 µm x 8 µm.

Figure 6 visualizes a registered image on the build plane. The original coaxial image is shown on the right. From the image frame registration work, it is known that this frame is registered at [-24.361 mm, 3.664 mm]. The calibrated temperature image is shown under the original. The dark red area has a temperature of over 2200°. The geometrical center of this area is assumed to be the laser spot center. The center pixel is marked in black color and located at row 60 column 70. The center pixel is registered to the [-24.361 mm, 3.664 mm]. The pixel represents an area of $\begin{bmatrix} -24.365\ \text{mm} & -24.357\ \text{mm} \\ 3.660\ \text{mm} & 3.668\ \text{mm} \end{bmatrix}$ in the plot of build platform coordinate system. The left figure shows the build platform coordinate system after registered all the pixels of this frame.

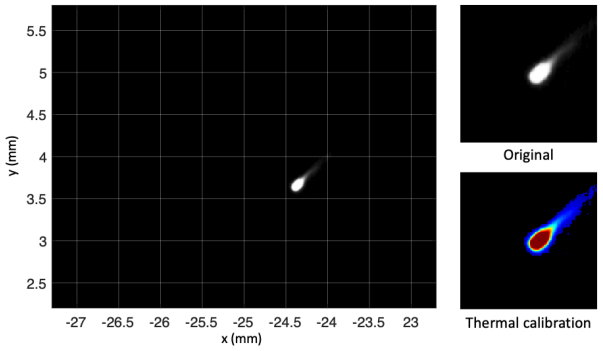

Figure 6: Coaxial image pixel registration example

Both an image frame and pixels are registered under uncertainties. The major uncertainty resources of the image frame registration are the signal delay and position variation. Figure 7 (a) and (b) plot the error distribution of the scan in x and y directions, respectively. The error is evenly distributed on both axes over the entire part. When registering an image frame using the related scan command, this uncertainty would be persisted. In this study, the real measured position is assumed to be the ground truth. However, it may include uncertainties from the measurement.

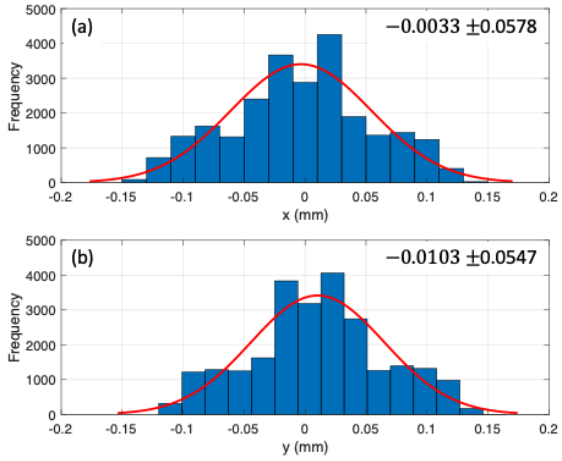

Figure 7. Statistical analysis for melt pool image registration. (a) and (b) are the distribution of error between real measurement and scan commands.

Image pixel registration combines the uncertainties from the previous step and the uncertainty initiated from the coaxial

images. First, the pixels registration refers to the frame position. The error of the position can be accumulated from pixel to pixel. Second, the pixel position depends on the laser spot found on the coaxial image, which is assumed to be closed to the image center. In this example, the image ($960\ \mu m \times 960\ \mu m$) center is at [480 µm, 480 µm]. However, the laser spot center is randomly distributed in a $100\ \mu m \times 100\ \mu m$ area at $[534 \pm 25, 454 \pm 23]$. The distribution is shown in Figure 8 as a heat map. The uncertainties analysis may be used for the optical and camera system adjustment.

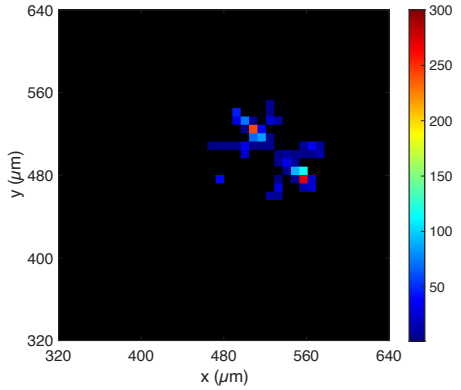

Figure 8. Heatmap of the center pixel frequency

4. CLOSED PBF SYSTEM CO-AXIAL MPM DATA REGISTRATION

4.1 Method overview

A closed AM system includes a commercial PBF machine as a base and many 3rd party addons such as in-situ monitoring systems. Because of the proprietary nature, most commercial AM machines don't give away the exact scan commands. Hence addon MPM system data registration is challenging because a 3rd party data acquisition is independent of the AM machine process control. And laser spot real position measurement during a build is seldom available to the users without breaking the warranty of the commercial machine. Hence the existing studies of melt pool characteristics and their correlations to other AM data are limited to layerwise global statistics because the laser spot positions for individual melt pool images are not available [14]. For this type of MPM systems, the real scan position for each melt pool has to be estimated based on machine-provided process settings and melt pool images themselves. This corresponds to Problem 1 for MPM data registration. Since Problem 2 for closed systems can be solved in a similar way in Section 3, it will not be discussed in this section.

As shown in Figure 9, a typical scan layer of a part is divided into contour region, hatching region, and skywriting region based on exposure strategy (laser power (P) and scan speed (v)) [22]. The contour region is an exposure area that creates the contour of a part, and a relatively small scale melt pool is formed due to low laser power and high scan speed. The hatching region is an exposure area that creates a core inside the contour of a part, usually using a higher laser power and a lower scan speed. Relatively large scale melt pools are formed in these regions. Figure 9 shows a stripe pattern for infill, one of the most frequently used scan strategies by commercial AM systems. The skywriting region is an unexposed area for scanner acceleration or de-acceleration in order to generate uniform energy density (P/v) in the hatch region. In this region, the melt pool is not formed because the laser is switched off.

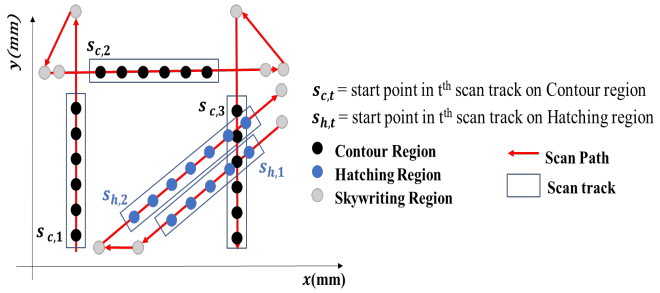

Figure 9: An example scan profile and scan regions

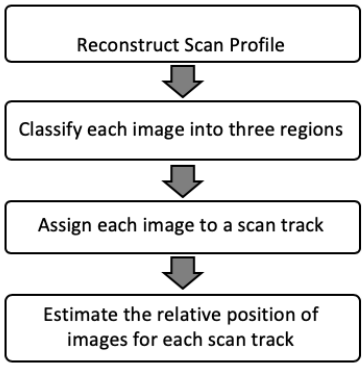

Figure 10: MPM data registration for closed systems

Figure 10 shows the overall workflow of the proposed MPM data registration method for closed AM systems based on the scan region definition.

1) A scan profile should be reconstructed from a process setting. Without losing generality, part contours, laser power for the contour (P_c), hatch pattern and direction (α), hatch distance (h_d), hatch laser power (P_h), and scanning speed (v) are given. With the process setting, a scan profile can be obtained, which is similar to Figure 9, including the contour(s) and hatch tracks.

2) Layerwise organized time series of melt pool images are classified into various regions. As shown in Figure 9, the melt pool images in the three regions are plotted as grey, black, and blue, respectively, in the figure. The details of the image classification will be discussed in the next sub-section.

3) The transient images are identified, e.g., from the skywriting region with "no melt pool" to the hatch region "with melt pool" or the other way around. These images correspond to the Start and End points of each scan tracks in a region, as grouped in the light blue rectangles in Figure 9. The start of a contour track is marked as $S_{c,t,}$ and that of the end point is marked as $E_{c,t.}$ Similarly, the start and end points of the hatch tracks are marked

as $S_{h,t,}$ and $E_{h,t}$. With the Start and End points identified, the images in between can be assigned to individual tracks.

4) Laser spot positions are assigned to the images, as shown in Figure 11. The corner points on the contour are assigned to the Start and End points on the contour tracks. The cross points of the contour and the hatch tracks identified in Step 1 are assigned to the Start and End points for the hatch tracks. For the images between the Start and End points on a trach, their positions can be obtained through linear extrapolation, from the position of previous melt pool image frame, the scan speed and sampling time shown in the equations below

$$\boldsymbol{x_{m+1,n}} = \boldsymbol{x_{m,n}} + \boldsymbol{t} \times \boldsymbol{v} \times \boldsymbol{cos(\alpha)} \quad (3)$$

$$\boldsymbol{y_{m+1,n}} = \boldsymbol{y_{m,n}} + \boldsymbol{t} \times \boldsymbol{v} \times \boldsymbol{sin(\alpha)} \quad (4)$$

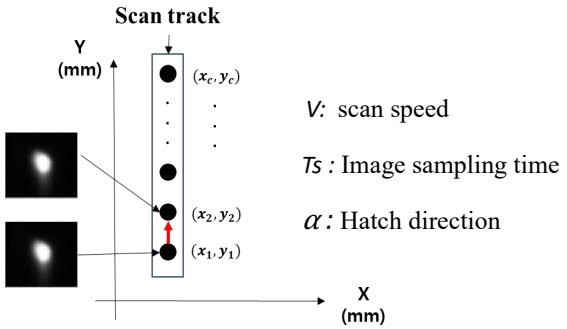

Figure 11: On-track image registration

4.2 Melt Pool Image Classification

The melt pool image can be classified based on the region because each region has a different exposure setting that determines the characteristics of the melt pool. In the skywriting region, no melt pool is taken in any images because the laser is turned off there. All pixel values of the image are zero and so can be easily distinguished. However, melt pool images in the regions with laser exposures, e.g., the contour region and the hatching region, are difficult to be separated by the pixel values due to various shapes of the melt pool, such as a long tail.

Because of differences with manufacturing conditions between 3rd parties, the rule-based methods of feature extraction, such as edge detection [25] and classification, cannot be used. To solve this problem, advanced machine learning algorithms are explored. To extract features of a melt pool image and classify whether the image is on a contour region or a hatching region, PCA and logistic regression are used respectively. PCA is a technique that finds latent variables orthogonal to each other while preserving the variance of data as much as possible and transforms variables from high-dimensional spaces into low-dimensional spaces without linear correlation [23]. Logistic regression is the most frequently used statistical model that obtains the probability value $P(\hat{Y})$ which is mapped to two classes (0 or 1) using a linear combination of input variables $x_1, x_2, \cdots, x_n$.(Equation (5)) [24]. Therefore, PCA is used to reduce high-dimensional image data (e.g., 61 pixel x 61 pixel = 3721) to low-dimensional data without linear correlation, and logistic regression is used to classify images into two types using the low-dimensional data as input variables.

$$\hat{Y} = \beta_0 + \beta_0 x_1 + \cdots + \beta_n x_n = \beta_0 + \sum_{i=1}^{n} \beta_i x_i \quad (5)$$

where $\hat{Y}$ is the predicted value, β_0 is the intercept and $\beta_1, \beta_2, \cdots, \beta_n$ are the coefficients which are estimated by maximum-likelihood. To deal with binary-classification, the real value of Y is transformed into the probability of Y occurrence with Equation 6.

$$P(\hat{Y}) = \frac{1}{1 + e^{-(\beta_0 + \sum_{i=1}^{n} \beta_i x_i)}} \quad (6)$$

4.3 Case study

This section presents a case study of the proposed method for closed-system MPM data registration. This study uses the melt pool images collected from NIST AMMT [17]; however, assuming the scan commands and laser spot positions unavailable. Instead, the scan command is used for algorithm validation. The measured laser spot position is not available for this set of data2

A layer with 2661 melt pool images is selected to validate the closed-system MPM data registration approach. Each image has a size of 128 pixels x 120 pixels at grayscale 0 to ≈255. The coaxial camera is triggered every 500 μs to collect melt pool image frames. To classify whether a melt pool image is on the contour or in the hatching region, a total of 2294 images are identified, with 60 images on the contour and 2134 images in the hatching region. 1720 images are used for training, and 574 are used as the test set for classification accuracy.

Table 1 is the scan profile of the NIST AMMT study [17].

TABLE 1: Scan profile of process parameters from NIST AMMT

Region type	Scan speed (mm/s)	Laser power (W)	Scan & Hatch direction(°)
Contour	900	100	{0,90,180,270}
Hatching	500,800	195	{67,247}
Skywriting	{0,...,900}	0	-

Figure 12 shows example images by region.

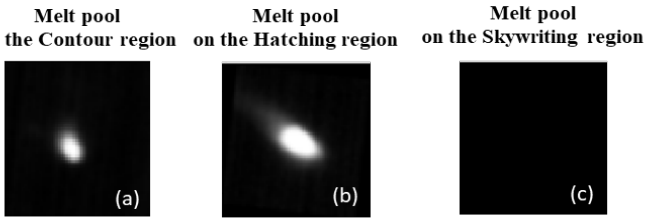

Figure 12: Example of melt pool image frame by region.

With 14 principal components resulted from PCA, Figure 13 shows two classified clusters with PCA and the result from logistic regression. Using the number of principal components of 14, the cumulative explained variance is 98%. With the 14 principal components of the training dataset, the classification accuracy of test sets is 99.65%.

As shown in Figure 13, the classification errors are those hatch track images mistakenly classified as contour images. Rules are built in the algorithm to automatically correct this type of error. The rule finally corrects 4 errors for the case study, which helps to avoid significant position estimation errors.

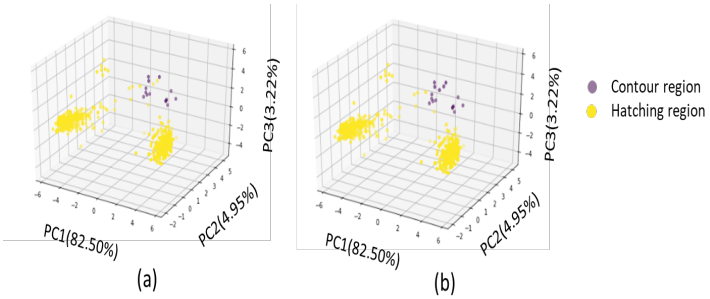

Figure 13: Plots of the logistic regression result in three principal axes. (a) is the result of the test dataset, and (b) is the predicted test dataset.

Figure 14 shows the MPM data registration using laser beam location estimation compared with the one registered against the build command. The top plot shows the registration against scan command, and the bottom plot shows the MPM data registration against the estimated positions using the proposed method. Both plots use the build platform coordinate system. The position error for all frames is less than 1 %.

The registration errors from the proposed laser spot position estimation methods come from 4 areas:

1) The scan profile reconstruction error
2) The laser spot position assigning error. Assigning the contour-hatch track cross point positions to the Start and End images on the hatch track could involve a position error as large as the laser travel distance within one image sampling time, about 400μm, for 500μs sampling time and 800mm/sec scan speed.
3) The algorithm assumes that there is no contour during the regular scan. The wrong assumption can cause significant classification error and translates to the position error.
4) The extrapolation error from nonlinear scan velocity

5. DISCUSSION AND FUTURE WORK

The objective of this work is to develop a generic data registration method and algorithms for camera-based coaxial melt pool monitoring for both open architecture AM systems and closed AM systems with 3rd part MPM additions. For an open AM system, each image taken by the coaxial MPM system is registered against the corresponding laser beam spot

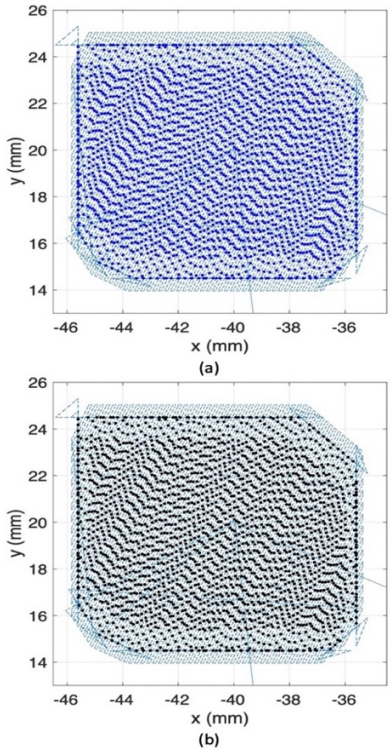

Figure 14: (a) MPM data registration against the scan command, and (b) MPM data registration against the estimated laser spot position

position based on synchronized camera trigger signals with the laser spot commands. The alignment between the melt pool images and the real laser positions can be made by getting rid of the delays introduced by the galvo position system and the camera control system. The delays can be measured during the calibration process. The individual image registration can be made based on the melt pool center identification and the calibrated camera pixel resolutions on the build plane. With the melt pool data accurately registered, 3D models can be reconstructed to correlate to the CAD model or post inspection data. The relationships will help in-situ part quality control and quality prediction. The machine learning-based laser spot position estimation method enables the MPM data registration for closed AM systems, which will benefit both the research labs and production facilities to enhance their integration capability at a lower cost. In the future, we will further improve the data registration method for closed AM systems for more complex scan patterns, by incorporating melt pool direction modeling to the on-track image position estimation. Deep learning methods will be explored for both image clustering and scan direction estimation. Deep dive uncertainty analysis will be conducted as well. For data interoperability and usability, these methods should be turned into standards. This requires us to work with the AM machine vendors and data users to further refine the data

registration methods. This is also one of the directions we are heading.

REFERENCES

[1]. Frazier, W. E., “Metal Additive Manufacturing: A Review”, Journal of Materials Engineering and Performance, (2014) 23:1917–1928, ASM International, DOI: 10.1007/s11665-014-0958-z

[2]. King, W. E., Anderson, A. T., Ferencz, R., 2015, "Laser Powder Bed Fusion Additive Manufacturing of Metals; Physics, Computational, and Materials Challenges," Applied Physics Reviews, 2(4) pp. 041304.

[3]. Fisher, B.A., Lane, B., Yeung, H., and Beuth, J., “Toward determining melt pool quality metrics via coaxial monitoring in laser powder bed fusion”, Manufacturing Letter, Manufacturing Letters 15 (2018) 119–121

[4]. Fox, J., Lane, B., and Yeung, “Measurement of process dynamics through coaxially aligned high speed near-infrared imaging in laser powder bed fusion additive manufacturing, Proc. SPIE 10214, Thermosense: Thermal Infrared Applications XXXIX, 1021407 (5 May 2017); https://doi.org/10.1117/12.2263863.

[5]. Grasso, M., Colosimo, B. M. “Process defects and in situ monitoring methods in metal powder bed fusion: a review,” Meas Sci Technol (2017), 28:044005. doi:10.1088/1361-6501/aa5c4f.

[6]. Yang, Z., Lu, Y., Yeung, H., and Krishnamurty, S., "Investigation of Deep Learning for Real-Time Melt Pool Classification in Additive Manufacturing," *2019* IEEE 15th International Conference on Automation Science and Engineering *(CASE)*, Vancouver, BC, Canada, 2019, pp. 640-647, doi: 10.1109/COASE.2019.8843291.

[7]. ISO 20005, “Information technology — Sensor networks — Services and interfaces supporting collaborative information processing in intelligent sensor networks”, https://www.iso.org

[8]. Hartley, R. and Zisserman, A., “Multiple View Geometry in Computer Vision”. Cambridge University Press, 2003

[9]. Chum, O., Pajdla, T., and Sturmb, P., “The geometric error for homographies”, Computer Vision and Image Understanding 97 (2005) 86–102

[10]. Brown, L. G., “A survey of image registration techniques”, ACM Computing Surveys archive, volume 24, issue 4, December 1992), pages 325 - 376

[11]. Villena-Martineza, V., Opreaa, S., Saval-Calvoa, M., Azorin-Lopeza, J., Fuster-Guilloa, A., and Fisherb, R. B., “When Deep Learning Meets Data Alignment: A Review on Deep Registration Networks (DRNs)”, https://arxiv.org/pdf/2003.03167.pdf, Accessed on May 7, 2020.

[12]. Zhirnov, I., Mekhontsev, S., Lane, B.M., and Grantham, S.E., “Accurate Determination of Laser Spot Position during Laser Powder Bed Fusion Process Thermography”, manufacturing Letters, Vol. 23 (2020) 49-52

[13]. Lane, B., and Yeung, Ho, “Process Monitoring Dataset from the Additive Manufacturing Metrology Testbed (AMMT): “Three-Dimensional Scan Strategies”, Journal of Research of the National Institute of Standards and Technology, Volume 124, Article No. 124033 (2019) https://doi.org/10.6028/jres.124.033

[14]. Yang, H. C., Adnan, M., Huang, C. H., Cheng, F. T., Lo, Y. L., and Hsu, C., H., “An Intelligent Metrology Architecture with AVM for Metal Additive Manufacturing”, IEEE Robotics And Automation Letters, Vol. 4, Issue 3, 2020.

[15]. ISO 841:2001, “ Industrial automation systems and integration — Numerical control of machines — Coordinate system and motion nomenclature”, https://www.iso.org

[16]. ISO 2806:1994, “Industrial automation systems — Numerical control of machines — Vocabulary”, https://www.iso.org

[17]. Lane, B. M., Mekhontsev, S., Grantham, S. E., Vlasea, M., Whiting, J. G., Yeung, H., Fox, J. C., Zarobila, C. J., Neira, J. E., McGlauflin, M. L., Hanssen, L. M., Moylan, S. P., Donmez, A. M., and Rice, J. P., “Design, Developments, and Results from the NIST Additive Manufacturing Metrology Testbed (AMMT)”, Proceedings of the Solid Freeform Fabrication, August 8-10, 2015, Austin, TX

[18]. Carter, W., Tucker, M., Mahony, M., Toledano, D., Butler, R., Roychowdhury, S., Nassar, A. R. , Corbin, D. J., Benedict, M. D., and Hicks, Adam S., “An Open-Architecture Multi-Laser Research Platform for Acceleration Of Large-Scale Additive Manufacturing (ALSAM)”, Proceedings of the 30th Annual International, Solid Freeform Fabrication Symposium, August 10-12, 2019, Austin, TX

[19]. Yeung H, Neira J, Lane B, Fox J, Lopez F (2016) Laser path planning and power control strategies for powder bed fusion systems. Proceedings of the 27th Annual International Solid Freeform Fabrication Symposium, Austin, TX. 113–127.

[20]. Li, Yajun. "Beam deflection and scanning by two-mirror and two-axis systems of different architectures: a unified approach." Applied optics 47, no. 32 (2008): 5976-5985.

[21]. Yang, Pei-Ming, Yu-Lung Lo, and Yuan-Hao Chang. "Laser galvanometric scanning system for improved average power uniformity and larger scanning area." Applied optics 55, no. 19 (2016): 5001-5007.

[22]. EoS, PSW software manual, 2008

[23]. Jolliffe, I.T., Principal Component Analysis. Springer-Verlag, 1986.

[24]. Hosmer, D. W., Lemeshow, S., and Sturdivant, R. X., Applied Logistic Regression, p. 1. John Wiley & Sons, third ed., 2013.

[25]. Sampson, R., Lancaster, R., Sutcliffe, M., Carswell, D., Hauser, C., & Barras, J. (2020). An improved methodology of melt pool monitoring of direct energy deposition processes. *Optics and Laser Technology*, *127*(December 2019).

[26]. Lane BM, Yeung H (2020) Process Monitoring Dataset from the Additive Manufacturing Metrology Testbed (AMMT): “Overhang Part X4.” *NIST Journal of Research (JRES)*. https://doi.org/(publication pending

[27]. NIST AMMT Datasets, https://www.nist.gov/el/ammt-temps/datasets

[28]. ISO/ASTM 52921, "Standard Terminology for Additive Manufacturing—Coordinate Systems and Test Methodologies", https://compass.astm.org/EDIT/html_annot.cgi?ISOASTM52921+13 (2019)